ELSEVIER

Catalysis Today 74 (2002) 249–256

CATALYSIS TODAY

www.elsevier.com/locate/cattod

Preparation of mesoporous silica fiber matrix for VOC removal

Young-Hwan Chu [a], Hyun-Jong Kim [a], Keun-Young Song [a], Yong-Gun Shul [a,*], Kyeong-Taek Jung [a], Kangtaek Lee [a], Moon-Hee Han [b]

[a] *Department of Chemical Engineering, Yonsei University, 134 Shinchon-Dong, Seodaemun-ku, Seoul 120-749, South Korea*
[b] *Korea Institute of Energy Research, P.O. Box 103, Yusung, Taejon 305-343, South Korea*

Received 28 September 2001; received in revised form 10 November 2001; accepted 30 November 2001

Abstract

A novel method for the preparation of the mesoporous silica fiber matrix was introduced for a removal of volatile organic compounds (VOCs). Paper making technology was applied to make a sheet of mesoporous silica fiber matrix. Reinforcing the mesoporous silica fiber with the ceramic fibers (50 wt.%) increased the mechanical strength of the matrix. Mesoporous silica fibers using TMOS (tetramethoxysilane) as a silica source and CTAC (cetyltrimethyl-ammoniumchloride) as a surfactant were drawn by the spinning method. The spinning process increased both the crystallinity and the fraction of mesopores (1.9 nm) of the fiber. As the spinning rate was increased both the crystallinity and the specific area of the mesoporous silica fiber increased, but the diameter of fiber decreased. We could control the size and morphology of mesoporous silica fiber matrix by changing the shape of substrates. This leads to easy fabrication of honeycomb-structured adsorbent which can be used for the VOC removal. © 2002 Published by Elsevier Science B.V.

Keywords: Mesoporous matrix; Mesoporous silica fiber; Paper making technology; VOC

1. Introduction

Volatile organic compounds (VOCs) are the most common pollutants and are considered as the significant atmospheric pollutants due to their toxicity and malodorous nature [1]. Major VOC emission sources include automobiles and various industries of organic chemicals, polymers, paints, and coatings [2]. Recently, a strict regulation on the environmental standards in several countries has initiated concerns on the pollutant controls and the VOC emission control is one of the major concerns in the environmental activities [3]. To date, thermal and catalytic oxidation, biological treatment, and the adsorption process have been used to remove VOCs. In the adsorption process, for instance, zeolite materials are mainly used as the adsorbents. However, in the case of zeolite materials, the relatively low gas hourly space velocity is a limiting factor for the VOCs adsorption system [4], and also the small pore size of zeolite materials could be problematic when large waste polymer molecules are emitted with VOCs in the real industries.

The most interesting feature of mesoporous materials is its regular pore structure, which consists of an hexagonal array with a pore dimension of 2–10 nm. This property offers a hope for the removal of VOCs molecules that are too large to fit in the pores of traditional zeolites [5,6]. In commercial the VOC removals using mesoporous materials, powders are usually converted to relatively large particulate forms by granulation or pelleting processes. In these cases, the diffusion rate and the adsorption capacity of VOCs in

* Corresponding author. Tel.: +82-2-2123-2758; fax: +82-2-312-6401.
E-mail address: shulyg@yonsei.ac.kr (Y.-G. Shul).

0920-5861/02/$ – see front matter © 2002 Published by Elsevier Science B.V.
PII: S0920-5861(02)00028-7

the mesoporous pellet decrease with the increase in the pellet diameter. To overcome this, it is necessary to change the morphology of the mesoporous materials into fibers or sheets. In our previous studies, we prepared the morphologically changed MFI-type zeolite fibers, films, and monoliths by using nano-technology and sol–gel analogy [7–11]. They showed a high diffusion rate with a low pressure drop in the reactor. Recently, we and some other groups reported a design of mesoporous materials with a controlled morphology by using inorganic/surfactant system [12–17]. In this study, we present a novel technique for the synthesis of mesoporous silica fibers and matrixes and also discuss their physico-chemical properties.

2. Experimental

2.1. Preparation of mesoporous silica fiber

Sol–gel process [17,18] was employed to prepare the mesoporous silica fibers. First, 9.71 g of tetramethoxysilane (TMOS) was partially hydrolyzed by 2.25 g of water (sub-stoichiometric amount) under acidic condition (pH = 3) for 2 h. This solution was dropped into a 20 g of the surfactant solution (cetyltrimethyl-ammoniumchloride, CTAC) with a vigorous stirring. The molar ratio of starting solution was TMOS:H_2O:CTAC = 4:8:1. After aging for 7 h, the viscous solution was transferred to a centrifugal spinning apparatus in which the temperature can be controlled. Mesoporous silica fibers were directly air-dried at 130 °C for 2 h in a drying chamber.

2.2. Mesoporous silica fiber matrix preparation

The mesoporous silica fibers were mixed with organic binders (i.e. pulp, PEG and PVA) in aqueous solution. The paper making process was applied to make a sheet of the mesoporous silica fiber matrix: the mixed solution was spread out in a substrate by filtration and was dried to prepare the sheet of uncalcined mesoporous matrix. To determine the effect of glass ceramic fiber on the mechanical strength, glass ceramic fibers were also added to the aqueous solution containing mesoporous fiber and organic binders. The uncalcined matrix was reinforced by colloidal silica solution, followed by thermal decomposition of organic materials at 650 °C for 5 h. Fig. 1 shows the experimental scheme of the preparation of the mesoporous matrix.

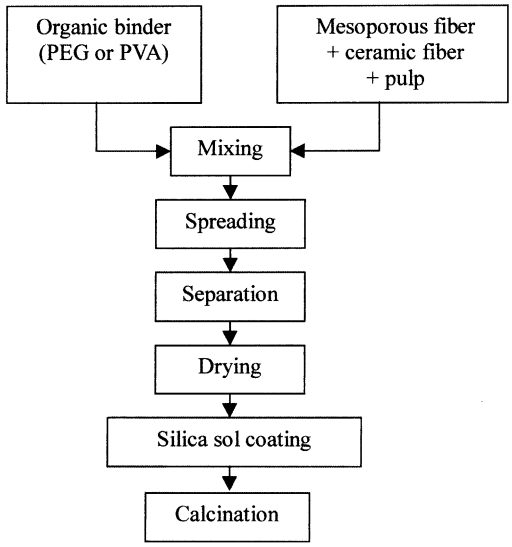

Fig. 1. Schematic representation for the preparation of mesoporous sheet.

2.3. Characterization

X-ray diffraction (XRD) patterns of fibrous mesoporous were obtained with a Cu Kα, X-ray source using a Rigaku instrument at room temperature. Scanning electron microscopy (SEM) images of the fibrous mesoporous materials were taken to show the surface and the cross-section with JEOL instrument. Nitrogen adsorption isotherms at 77 K were measured with a SORPTOMATIC 1990, FISONS. Each sample was pre-treated at 500 °C for at least 12 h until a pressure of 10^{-2} Pa was achieved.

Temperature programmed desorption (TPD) of ammonia was carried out to evaluate the acidic properties of the fibrous mesoporous materials using NH_3 as an adsorbate. The 0.02 g of a calcined sample was placed in a quartz reactor and heated at 500 °C under vacuum for 9 h. The reactor was then cooled to room temperature and the NH_3 gas was passed over the sample for 1 h. The sample was kept in the vacuum at room temperature for 1 h to eliminate the physisorbed ammonia. The desorption of NH_3 and the acid strength

distribution of the samples were obtained by raising the temperature at 3 °C/min. TPD of toluene was also carried out using the same method.

3. Results and discussion

During the preparation of acid/surfactant spinning sol, the alkoxide solution is clear and typically stable for several hours. After 7 h, the solution eventually becomes viscous showing the optimum viscosity for the fiber spinning rather than the formation of silica particles, as in the acid-route synthesis of Huo et al. [19].

Fig. 2 shows the XRD pattern of (a) as-synthesized bulk, (b) the fiber after spinning process, and (c) the calcined mesoporous silica fiber at 600 °C. All patterns are similar and they exhibit typical low angle (1 1 0) diffraction associated with the nature of mesoporous silica [20]. Analogous diffraction patterns have been observed for hexagonal mesostructures prepared by electrostatic or neutral templating pathways [20,21]. The as-synthesized before spinning bulk phase sample shows rather broad diffraction peak (centered at $2\theta = 2.10^\circ$, d_{100} value = 4.1 nm). After spinning process the fibrous sample obtained by spinning process shows sharper diffraction peak and the main peak is shifted to higher angle (centered at $2\theta = 2.21^\circ$, d_{100} value = 4.0 nm). The d_{100} value of mesoporous material was decreased from 4.1 to 4.0 nm and the scattering intensity increased substantially. This suggests that the spinning process induces the lattice contraction and also promotes the ordering of the mesoporous materials. After calcination, the scattering intensity of the sample increased. A lattice contraction of 22.5% is also observed as the d_{100} spacing decreases to 3.1 nm.

Fig. 3 shows SEM micrographs of (a) the surface and (b) cross-section of the mesoporous silica fibers prepared from TMOS/CTAC at 130 °C at a spinning rate of 1000 rpm. The silica fiber is 50 μm in diameter with a circular shape. Fig. 4 shows the optical microphotograph of mesoporous hair-like fiber calcined at 600 °C for 1 h. The fiber is a few centimeters long and optically transparent. This may come from the high degree of ordering on the micrometer length scale. The mesoporous silica fibers become slightly brittle after: calcination because of the removal of surfactants.

Fig. 5 shows the effect of spinning rate (rpm) on the XRD patterns. All the samples were calcined at 600 °C for 1 h. The arbitrary intensity of XRD increases dramatically from 1335 to 5023 as the spinning rate is increased. This suggests that the spinning rate affects the ordering or the *c*-axis orientation of mesopore which

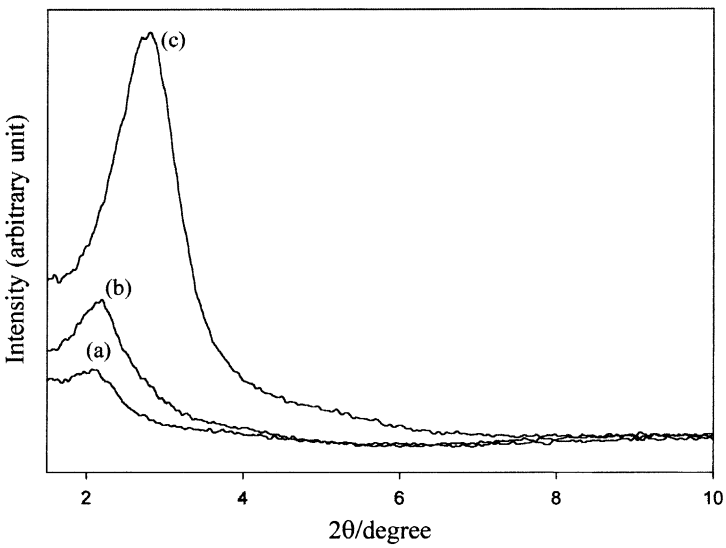

Fig. 2. XRD patterns of the mesoporous materials: (a) as-synthesized bulk phase; (b) before spinning fiber; (c) after spinning (1000 rpm) fiber calcined at 600 °C for 1 h.

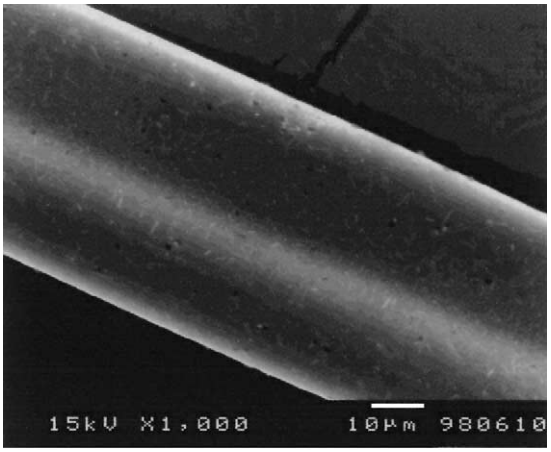

(a)

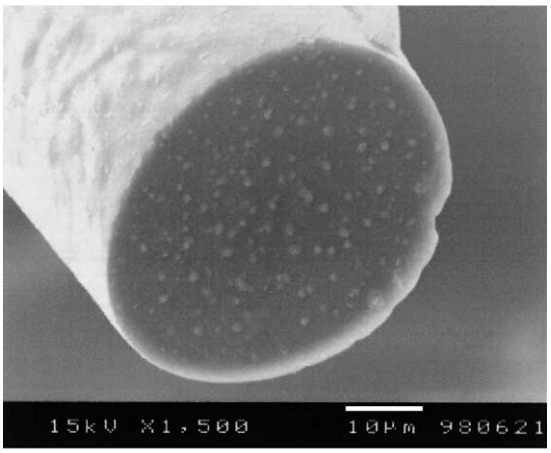

(b)

Fig. 3. SEM image of fibrous mesoporous materials: (a) surface; (b) cross-section.

was prepared by the surfactant micelle as template and silica alkoxide as silica precursor in the mesoporous silica fiber because the high centrifugal force. Table 1 shows the effect of spinning rate on the specific BET area and the diameter of mesoporous silica fiber. The specific surface area of mesoporous silica fiber increases from 547 to 605 m^2/g and the diameter of the mesoporous fiber decreases from 80 to 20 μm as the spinning rate is increased from 500 to 2000 rpm. The increase in the BET surface area of the fibers may result from the decrease of fiber diameter. During the spinning and the calcination processes, the water and organic materials evaporate more readily from the thin fiber: in the thinner fibers, the water and organic materials evaporate at lower temperature and also more homogeneously than in the thicker fibers. The BET surface area can be increased by the evaporation of water and/or organic materials at high spinning rate. We speculate that it should promote the ordering of organic template in silica matrix.

Table 1
Effects of the spinning speed on the physical properties of the mesoporous silica fiber

Spinning speed (rpm)	500	1000	2000
Fiber diameter (μm)	80	50	20
Specific surface area (m^2/g)	547	586	605
Relative crystallinity: (XRD peak intensity of sample)/(XRD peak intensity of 2000 rpm sample)	0.575	0.717	1

Fig. 6 shows the effect of spinning rate on the Horvath–Kawazoe (HK) pore size distribution of the mesoporous silica fibers. At higher spinning rate, the secondary pores of 20–25 Å developed, which may suggest that the spinning rate affects the growth of mesopore structure. The pore size distribution for this material is very similar to that of MCM-41 with a poor structural order [22,23]. It suggests that the first peak can be assigned to the pore in the amorphous silica. The second peak size is similar to that of the other mesoporous materials using the same organic template (CTAC) [13,17].

Fig. 7 shows the optical microphotograph of mesoporous silica fiber matrix. The diameter is about 10.5 cm and the shape is circular. We can easily control the shape and size of mesoporous matrix by changing the filtering area and the shape in paper making process. Table 2 shows the mechanical strength of mesoporous sheet with the addition of ceramic fiber. Sample 2 consists of 50:50 mixture of the

Table 2
Mechanical strength of mesoporous sheets

Sample number	Ceramic fiber: mesoporous fiber	Strain at yield (%)	Yield strength (kg_f)
1	100:0	3.127	3.013
2	50:50	2.369	2.292
3	0:100	1.591	1.603

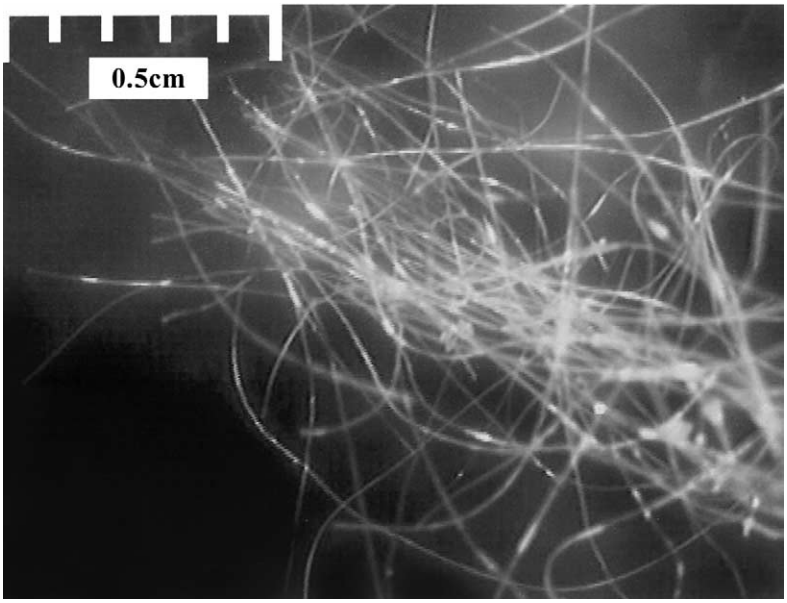

Fig. 4. Optical microphotograph of fibrous mesoporous materials.

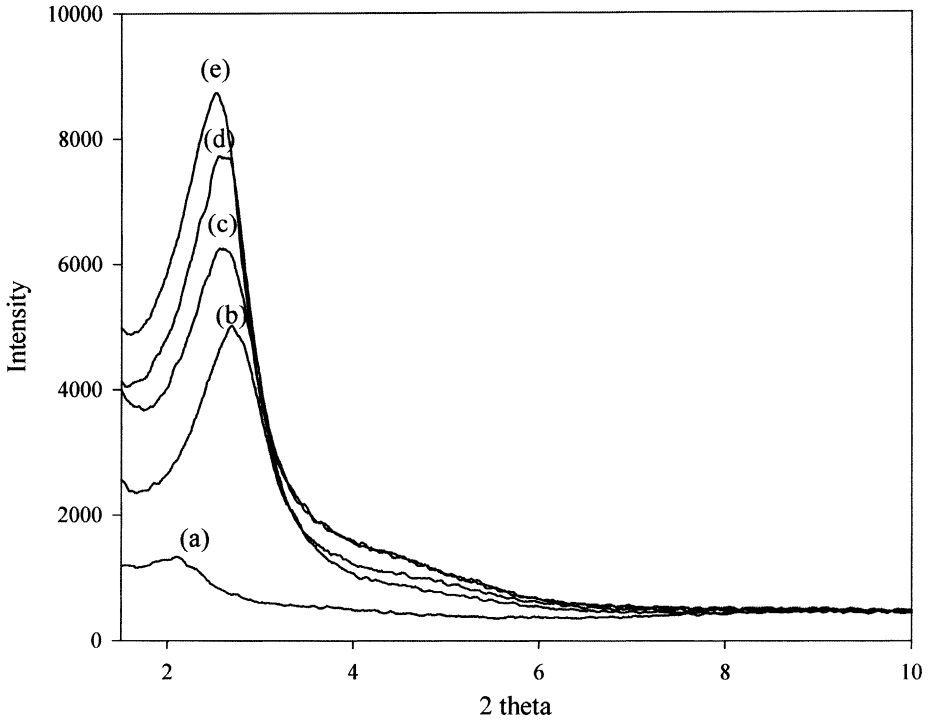

Fig. 5. Effect of spinning rate on the XRD pattern: (a) bulk phase; (b) 500 rpm; (c) 1500 rpm; (d) 2000 rpm; (e) 2500 rpm.

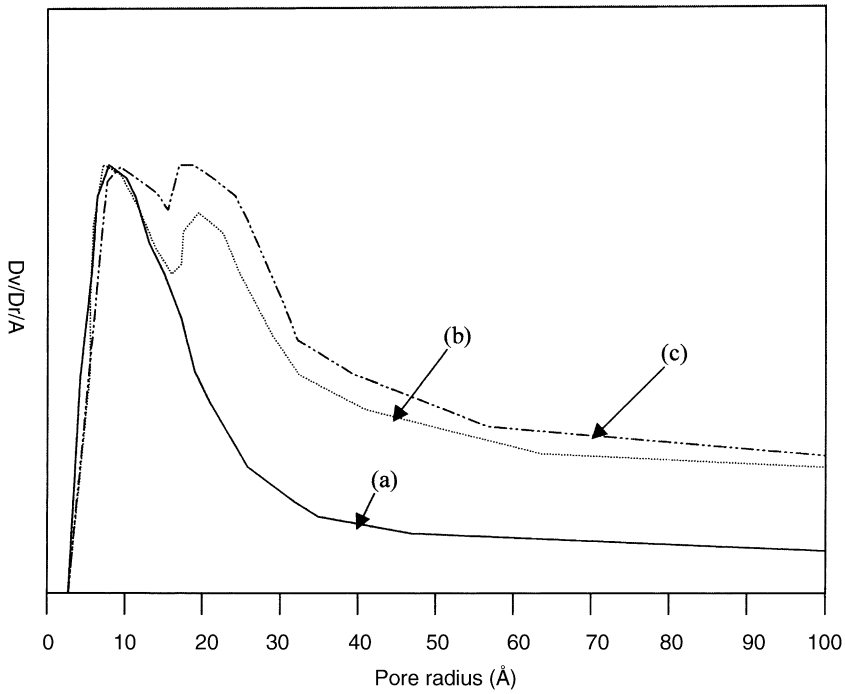

Fig. 6. Pore size distribution of mesoporous fibers at various spinning rates: (a) bulk powder; (b) 1500 rpm; (c) 2000 rpm.

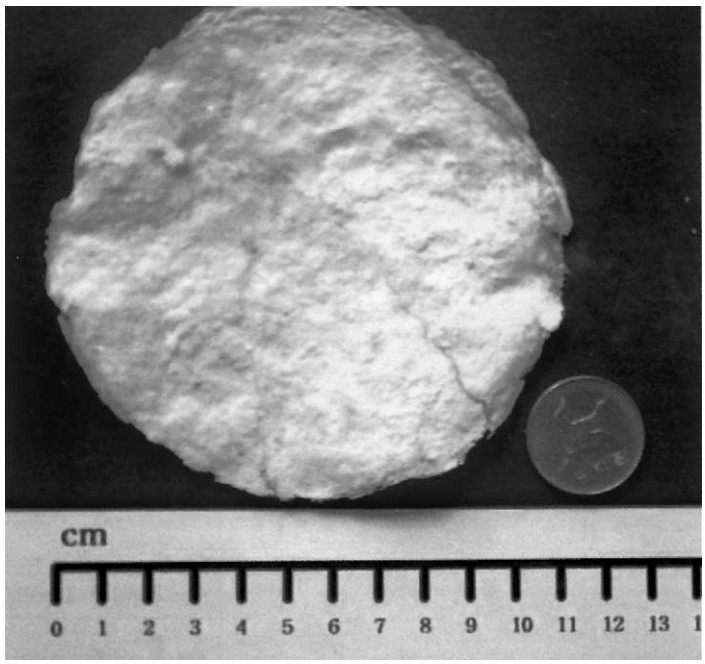

Fig. 7. Optical microphotographs of mesoporous sheet.

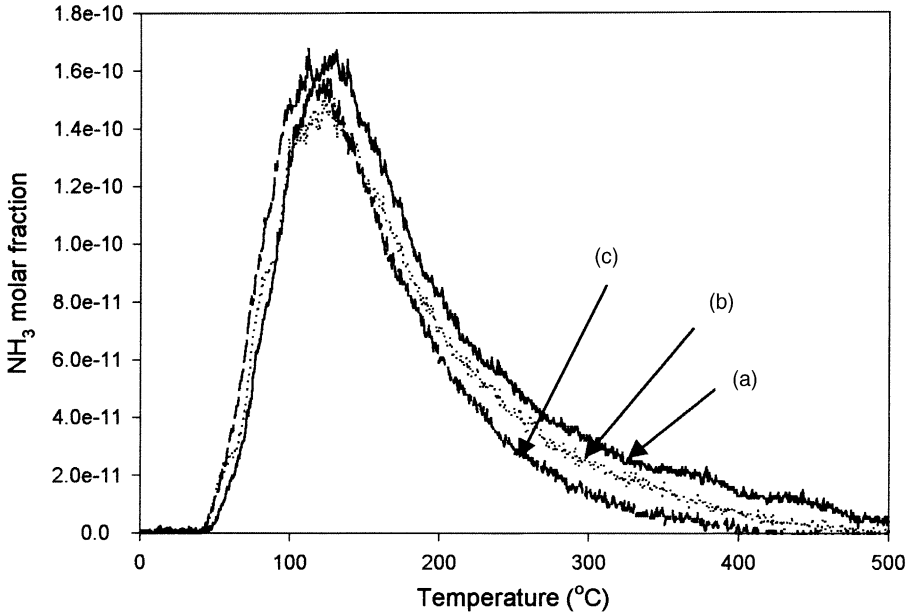

Fig. 8. NH_3-TPD spectra of mesoporous materials: (a) mesoporous bulk powder; (b) mesoporous fiber (500 rpm); (c) mesoporous fiber (2500 rpm).

ceramic and mesoporous fiber while sample 3 consists of the pure mesoporous silica fiber. The strain at yield point of samples 2 and 3 is 2.369 and 1.591%, respectively. If we introduce the silica fiber in the aqueous solution containing mesoporous silica fiber and organic binder, both the strain at yield and the yield strength are higher than those of the 100% mesoporous silica fiber sample. The 50% reinforcement

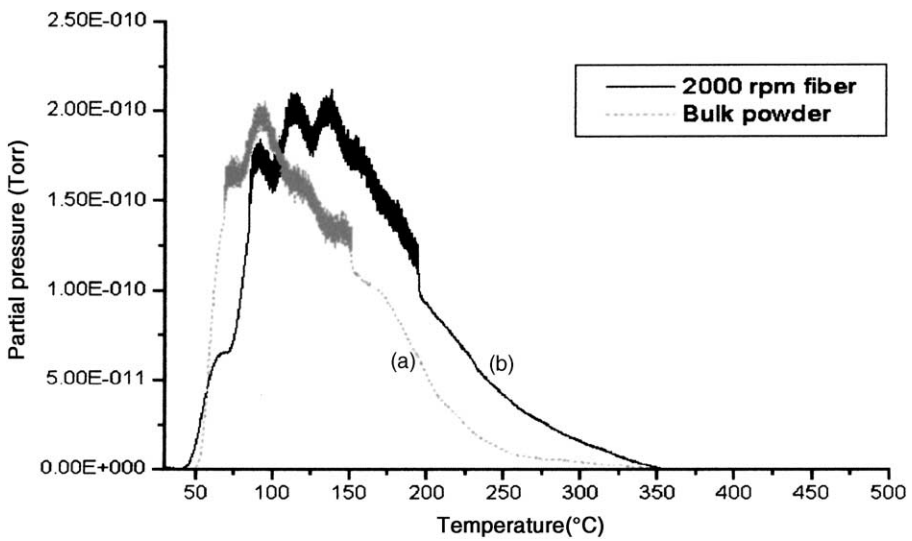

Fig. 9. Toluene-TPD spectra of mesoporous materials: (a) bulk phase before spinning; (b) mesoporous fiber (2000 rpm).

of the ceramic fiber seems to be enough to make a honeycomb-structured of mesoporous silica fiber matrix for the VOC removal.

Fig. 8 shows ammonia TPD spectra of (a) the bulk powder, (b) the mesoporous silica fiber obtained at 500 rpm, and (c) the mesoporous silica fiber obtained at 2500 rpm. All of them show the similar profiles of ammonia desorption, indicating a similarity in acidity. The intensity of the desorption peak at high temperature (>200 °C) is slightly reduced at higher spinning rate, and the adsorption capacity is decreased. This suggests that the strength of the surface acid sites is decreased with the increase in the spinning rate. Fig. 9 shows toluene-TPD spectra of the as-synthesized bulk and the mesoporous silica fiber. The adsorption capacity of toluene slightly increased after the spinning process and the maximum desorption peak is shifted to higher temperature. The adsorption of aromatic hydrocarbon in the silica mesoporous materials results from the weak interaction of the π-electrons of the aromatic ring with the terminal silanol group which is poorly acidic or nonacidic. Bulk powder has only one desorption peak at 92 °C, whereas the mesoporous silica fiber shows two desorption peaks at 114 and 137 °C. Two desorption peaks shown in the mesoporous silica fiber are maybe due to the pore diffusion effect induced by the existence of two kinds of channels, one is 1 nm, and the other 2 nm, as shown in pore size distribution data in Fig. 6 [24] and due to the generation of new adsorption site generated by the spinning process [25].

4. Conclusions

The mesoporous silica fiber matrix was successfully prepared using the paper making technologies. XRD patterns and the pore size distribution of the mesoporous silica fibers were very similar to those of MCM-41 with a somewhat poor structural order. The mesopore structured was evolved as increasing the spinning rate of spinning apparatus. Finally, these mesoporous materials can be prepared as sheet form to remove VOCs in atmosphere.

References

[1] J.A. Horsley, Catalytica Environmental Report No. E4, Catalytica Studies Division, Mountain View, CA, 1993.
[2] C.M. Edward, N. Mukhopadhyay, VOC Control: Current Practices and Future Trends, Chemical Engineering Progress, July, 1993.
[3] M. Kosusko, C.M. Nunez, J. Air Waste Manage. Assoc. 40 (1990) 254.
[4] S. Kawi, M. Te, Catal. Today 44 (1998) 101.
[5] C.T. Kresge, M.E. Leonowicz, W.J. Roth, J.C. Vartuli, J.S. Beck, Nature 359 (1992) 710.
[6] Q. Huo, D.I. Margolese, G.D. Stucky, Chem. Mater. 8 (1996) 1147.
[7] K.-T. Jung, Y.-G. Shul, Micropor. Mesopor. Mater. 21 (1998) 281.
[8] K.-T. Jung, H.-J. Kim, Y.-G. Shul, D.S. Kim, J.K. Kim, Stud. Surf. Sci. Catal. 105 (1997) 2241.
[9] K.-T. Jung, Y.-G. Shul, Chem. Mater. 9 (1997) 420.
[10] K.-T. Jung, H.-J. Kim, Y.-G. Shul, K.K. Koo, AIChE J. 43 (1997).
[11] K.-T. Jung, H.-J. Kim, Y.-G. Shul, D.S. Kim, Zeolites 19 (1997) 161.
[12] K.-T. Jung, Y.-H. Chu, Y.-G. Shul, Non-Cryst. Solids, submitted for publication.
[13] S.H. Tolbert, T.E. Schaffer, J. Feng, P.K. Hansma, G.D. Stucky, Chem. Mater. 9 (1997) 1962.
[14] M.C. Weissenberger, G.C. Goltner, M. Antonietti, Berichte Bunsen Gesellschaft (Phys. Chem. Chem. Phys.) 101 (1997) 1679.
[15] Q. Huo, J. Feng, F. Schuth, G.D. Stucky, Chem. Mater. 9 (1997) 14.
[16] M. Ogawa, Chem. Commun. (1996) 1149.
[17] P.J. Bruishman, A.Y. Kim, J. Liu, S. Baskaran, Chem. Mater. 9 (1997) 2507.
[18] C.J. Brinker, G.W. Scherer, Sol–Gel Science: The Physics and Chemistry of Sol–Gel Processing, Academic Press, San Diego, CA, 1990.
[19] Q. Huo, B. Xianhui, P. Feng, T.E. Gier, G.D. Stucky, Chem. Mater. 6 (1994) 1176.
[20] C.Y. Chen, H.Y. Li, S.L. Burkett, M.E. Davis, Micropor. Mater. 2 (1993) 27.
[21] P.T. Tanev, T.J. Pinnavaia, Science 267 (1995) 865.
[22] A. Corma, V. Fornes, M.T. Navarro, J. Perez-Pariente, J. Catal. 148 (1994) 569.
[23] J.M. Kim, C.H. Shin, R. Ryoo, Catal. Today 38 (1997) 221.
[24] M.J. Lee, S.W. Nam, W.Y. Lee, H.K. Rhee, B.P. Sung, Hwahak Konghak 25 (1987) 71.
[25] Y.A. Saleh-Alhamed, R.R. Hudgins, P.L. Silveston, Appl. Catal. A 125 (1995) 177.